Eur. Phys. J. D **8**, 169–176 (2000)

THE EUROPEAN PHYSICAL JOURNAL D

EDP Sciences

Line emission and alignment effects in state selective electron transfer in He^{2+}–Li(2s, 2pΣ, 2pΠ) collisions

A.N. Perumal and D.N. Tripathi[a]

Department of Physics, Banaras Hindu University, Varanasi 221 005, India

Received 3 July 1998 and Received in final form 3 June 1999

Abstract. Classical Trajectory Monte-Carlo (CTMC) method has been used to investigate state selective electron capture by He^{2+} ions colliding with Li($2s$) and $Li^*(2p)$ in Σ as well as Π alignments in the energy range 1–15 keV/amu. $He^+(4l)$ electron capture, line emission [He II($n = 4 \rightarrow 3$)] cross-sections and alignment parameters have been calculated and analyzed in the light of the available results. The undulatory structure of the capture and emission cross-sections have been explained qualitatively in terms of a quasi-molecular ion formation. Projectile impact energy and spatial overlap play crucial role in determining the alignment effects.

PACS. 34.70.+e Charge transfer

1 Introduction

The line emission cross-sections for single/multiple charged ions colliding with Li($2s$) atom have been extensively studied [1–7] not only due to its importance on fundamental aspects but also because of its applications in modeling and diagnostic studies of magnetically confined (tokamak) nuclear fusion plasmas [8,9]. The observation of the visible line radiation following electron capture collisions by plasma constituents from the neutral beam atoms provides critical information about impurity ions concentrations and their velocity distributions. Besides spherically symmetric ground-state target atoms, orbital-alignment-dependent collisions can provide additional insight into dynamical processes [10].

Recently Hoekstra *et al.* [2] determined the capture cross-section using the measured line emission cross-sections for He II($n = 4 \rightarrow 3$) transitions in He^{2+}–Li($2s$) collisions and compared them with the Atomic Orbital (AO) calculations of Fritsch and Lin [11] as well as the experimental results of Aumayr *et al.* [12]. A critical evaluation reveals that the claimed agreements are, in general, not convincing. For example, Hoekstra *et al.*'s observed line emission cross-sections for He II($4 \rightarrow 3$) transition are appreciably less as compared to the AO and Aumayr *et al.*'s corresponding results. Similarly, in case of nl ($4s, 4p, 4d$ and $4f$) capture cross-sections the agreement with AO as well as experiment is also not that satisfactory. Further work therefore, to explain the observed features of the capture and line emission cross-sections particularly, the oscillations in the total and lower l partial cross-sections appears to be essential. Also, as mentioned above, the atom in its excited state with its electron orbits aligned is expected to provide useful informations and throw further light regarding electron transfer processes and decay of the final capture state.

Although, cross-section measurements characterize production from a reaction channel, informations regarding the shape of the charge cloud are not transparent from it since the procedure effectively averages over the final electronic configurations [13]. The knowledge of *dimensionless* parameters A and R, as defined in reference [14], are therefore, essential in understanding of alignment effects on the capture process. The orbital alignment effects in case of $Na^*(3p)$ colliding with single/multiple charged ions have been studied by several workers [13–18]. Gieler *et al.* [18,19] investigated it in case of $Li^*(2p)$ and $Na^*(3p)$ aligned targets theoretically (Atomic Orbital calculation) as well as experimentally in which they determined the final n distributions of the cross-section and alignment effects on it.

In the present work we have calculated nl sublevel capture and line emission cross-sections in the incident energy range of 1 to 15 keV/amu for He^{2+}–Li($2s$, $2p\Sigma$, $2p\Pi$) systems. Capture cross-sections have been simulated using the CTMC method. Line emission cross-sections are determined using the calculated partial capture cross-sections to a specific principal and orbital angular momentum quantum number level (nl) and the corresponding branching ratios. *Dimensionless* parameters R and A have also been determined and the alignment effects have been discussed in terms of these parameters.

[a] e-mail: dnt@banaras.ernet.in

2 Theory

The three body CTMC method used here has been described earlier in detail [20,21] and therefore, only essential points particular to this work are described. The Li($2s$, $2p$) electron is assumed to move in a model potential of the form [22]

$$V(r) = -\frac{1}{r}[(Z-z)\mathrm{e}^{-Ar} + Br\mathrm{e}^{-Cr} + z] \qquad (1)$$

where Z is the atomic charge, z is the net charge seen by the electron far from the nucleus and A, B and C are constants. The shape of the electron charge cloud has been initialized by fixing the magnetic angular momentum quantum number in an appropriate value [23,24]. In case of the Li$^*(2p)$ target two kinds of alignments have been considered *viz.*, the electron orbital plane oriented parallel ($m = 0$) and perpendicular ($m = 1$) to the incoming ion direction defined as the axis of quantization **z**. The parallel and perpendicular alignments of Li$^*(2p)$ target are denoted as $2p\Sigma$ and $2p\Pi$ states respectively. The final test for the capture process are carried out at the end of individual trajectory far away from the interaction region. The principal quantum number n of the captured electron is determined by defining a classical number n_c based on the binding energy E_p of the electron relative to the projectile, *viz.*;

$$E_\mathrm{p} = -\frac{Z_\mathrm{p}^2}{2n_\mathrm{c}^2} \qquad (2)$$

where Z_p is the projectile charge. The final state n is obtained from the classical n_c *via* the condition [25]

$$[(n-\frac{1}{2})(n-1)n]^{1/3} \leq n_\mathrm{c} < [n(n+\frac{1}{2})(n+1)]^{1/3}. \qquad (3)$$

The angular momentum l of the final state is determined from the classical angular momentum l_c *via*

$$l \leq l_\mathrm{c} < l+1 \qquad (4)$$

where $l_\mathrm{c} = (n/n_\mathrm{c})(\mathbf{r}\times\mathbf{p})$, with **r** and **p** the position and velocity vectors of the electron with respect to the projectile core. In order to get a meaningful results for the sublevel and total capture cross-sections, 10^4 to 10^5 trajectories (depending upon the projectile energy) were computed at each energy.

3 Results and discussion

3.1 Capture cross-section

3.1.1 He^{2+}–Li(2s)

Figure 1 shows the He II($n = 3, 4, 5$) capture cross-sections along with the experimental results of Hoekstra *et al.* [2], Aumayr *et al.* [12] and the combined experimental and theoretical results of Gieler *et al.* [19]. The present CTMC results underestimates the Gieler *et al.* and Aumayr *et al.*'s cross-sections for $n = 3$ level at low energies. However, at high energies the available results are reproduced satisfactorily by the present CTMC calculations.

The He II($n = 4$) capture cross-sections are shown in the same Figure 1 along with the results of Hoekstra *et al.* [2], Aumayr *et al.* [12] and Gieler *et al.* [19]. The trend of the variation of the CTMC capture cross-section with incident energy is in good agreement with the Hoekstra *et al.*'s and Aumayr *et al.*'s observed results. The AO calculation result of Gieler *et al.* however, overestimate all the other cross-sections in the high energy region.

The CTMC capture cross-sections for He II($n = 5$) shows an excellent agreement with the measured results of Gieler *et al.* and Aumayr *et al.* However, the results of AO calculation of Gieler *et al.* show some discrepancy with all the available results particularly, in the energy region above 4 keV/amu. Among the different partial cross-sections, $n = 5$ channel contains large number of undulations. These undulations would be discussed later on in the subsequent section.

The nl distributions of the capture process depend on the relative importance of the radial and rotational couplings, on the Stark mixing and the projectile core electrons effect. In the case of fully stripped ions colliding with lithium atoms, all nl sublevels (n fixed) are affected by the Stark effect due to the Li^+ residual ion. The capture to the states with large l values being favored, these states are populated by single-electron capture [26]. We have calculated all the sublevel cross-sections but presenting only the $4l$ cross-sections as comparable results are available only for this case. Amongst the He$^+(4l)$ sublevels, $4f$ is the dominant one which corroborates the above fact. The CTMC $4s$ capture cross-sections are shown in Figure 2a along with the measured result of Hoekstra *et al.* [2] and the AO calculation of Fritsch and Lin [11]. The trend of the present result is in better agreement with that of Hoekstra *et al.* The magnitudes are however, almost half that of the Hoekstra *et al.*'s results. The observed cross-sections for $4s$ sublevel are likely to have been enhanced due to the cascading of states *viz.*; $5g \rightarrow 4f \rightarrow 3d$. In the experiment, sublevel capture cross-sections are obtained out of the measured line emission cross-sections after a deconvolution based on their life times. It would be difficult to distinguish amongst $4s$ and $5g$ levels resolutely as the two have their life times almost the same. In view of the above mentioned fact the observed $\sigma(4s)$ capture cross-sections are compared with the apparent $4s$ cross-section calculated as [2]

$$\begin{aligned}\sigma^*(4s) &= \sigma(4s) + \left(\frac{\tau_{4s}}{b_{4s}}\right)\left(\frac{b_{5g}}{\tau_{5g}}\right)\sigma(5g) \\ &\approx \sigma(4s) + 2.35\sigma(5g) \end{aligned} \qquad (5)$$

where τ_{4s} and τ_{5g} are the life times of the $4s$ and $5g$ levels (14.2 and 14.5 ns respectively), and b_{4s} and b_{5g} are, respectively the branching ratio for $4s \rightarrow 3p$ transition (0.42) and the total branching ratio (1.0) for the cascade $5g \rightarrow 5d \rightarrow 3p$. This calculated cross-sections are found

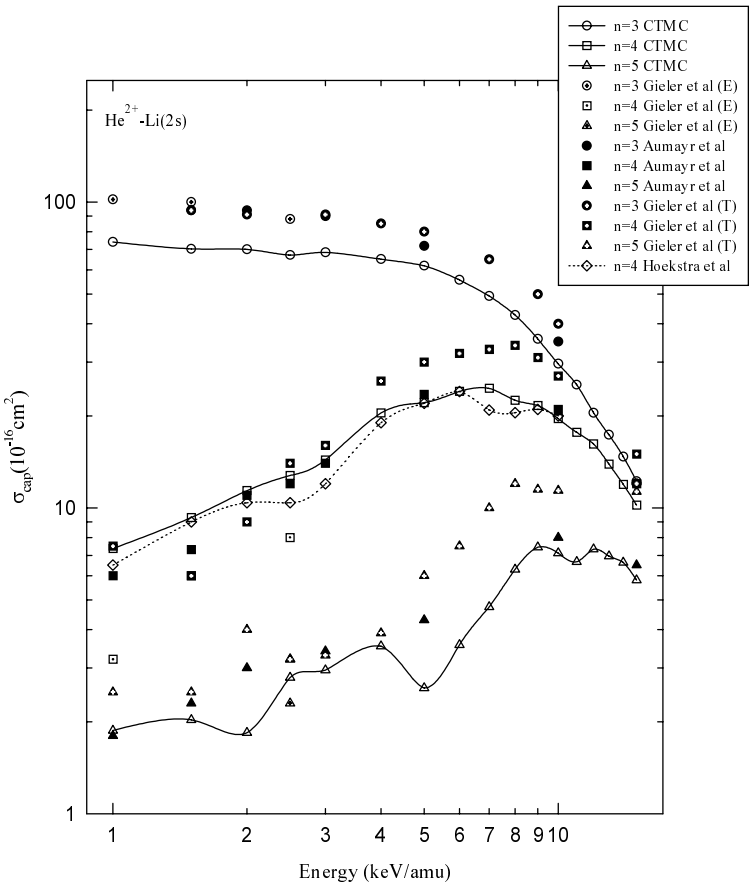

Fig. 1. Electron capture cross-section into $He^+(n = 3, 4, 5)$ (E and T denotes the experiment and theoretical results of Gieler *et al.* respectively).

to be in excellent agreement with the experimental results of Hoekstra *et al.* [2] (see Fig. 2a). The capture cross-sections reported by Fritsch and Lin are not in agreement with that of the present as well as experimental results. CTMC cross-sections for the $4p$ sublevel have been compared with the AO calculation of Fritsch and Lin [11] and the experimental results of Dijkkamp *et al.* [27] (see Fig. 2b). Both AO as well as CTMC calculations underestimate the experimentally determined cross-sections. The trend of the CTMC and AO results are in good agreement with each other. The $4d$ sublevel cross-sections are in fair agreement with the measured and AO results (Fig. 2c). Hoekstra *et al.*'s cross-sections are over estimated by both the CTMC as well as AO calculations below 4 keV/amu. All the reported cross-sections resembles with the present results in the high energy region. The $4f$ state partial cross-sections are in an excellent agreement with AO results but are larger than the experimental results (Fig. 2d). In experiment, as mentioned above it is the line emission cross-section which is basically measured and is converted into the sublevel capture cross-sections using the corresponding branching ratios. The measured line emission cross-section for $4f$ state is lower than all the other results and therefore, the magnitude of the $4f$ cross-section (since branching ratio for $4f$ is 1.0) is naturally low. The trend of the $4f$ state capture cross-sections curve however, is in good agreement with our CTMC results.

3.1.2 He^{2+}–$Li^*(2p\Sigma, 2p\Pi)$

In order to examine the orbital alignment effects on the total and sublevel capture cross-sections, the collision of He^{2+} with excited $Li^*(2p)$ having Σ and Π alignments have been studied and the results are shown in Figures 3a–3d. The capture cross-sections from $Li^*(2p\Sigma)$ and $Li^*(2p\Pi)$ initial states differ appreciably. The cross-sections from Π initial state is dominant over that of Σ in case of $4f$ and $4d$ final states whereas, it is the capture from Σ that dominates if the final capture state is $4s$. In case of $4p$, both the cross-sections are almost the same. In case of $4f$ sublevel, capture cross-section from the $Li^*(2p\Pi)$ target state is larger than that of the $Li^*(2p\Sigma)$ state in the energy region below 6 keV/amu. Above 7 keV/amu it is just the reverse. The cross-sections from both the symmetries at ~ 6.5 keV/amu *i.e.*, at the velocity matching energy are the same. The strong preference for the Π state at low energies can be attributed to an orbital overlap in x space of the $2p\Pi$ state with the projectile's trajectory. The decrease in preference at velocities approaching the $2p$-electron classical velocity is due to a decrease in overlap of the participating wave functions in velocity space. In contrast to this situation, in case of Σ state the overlap in velocity space does not change significantly due to the electron's motion being preferentially along the ion beam direction and this is the reason

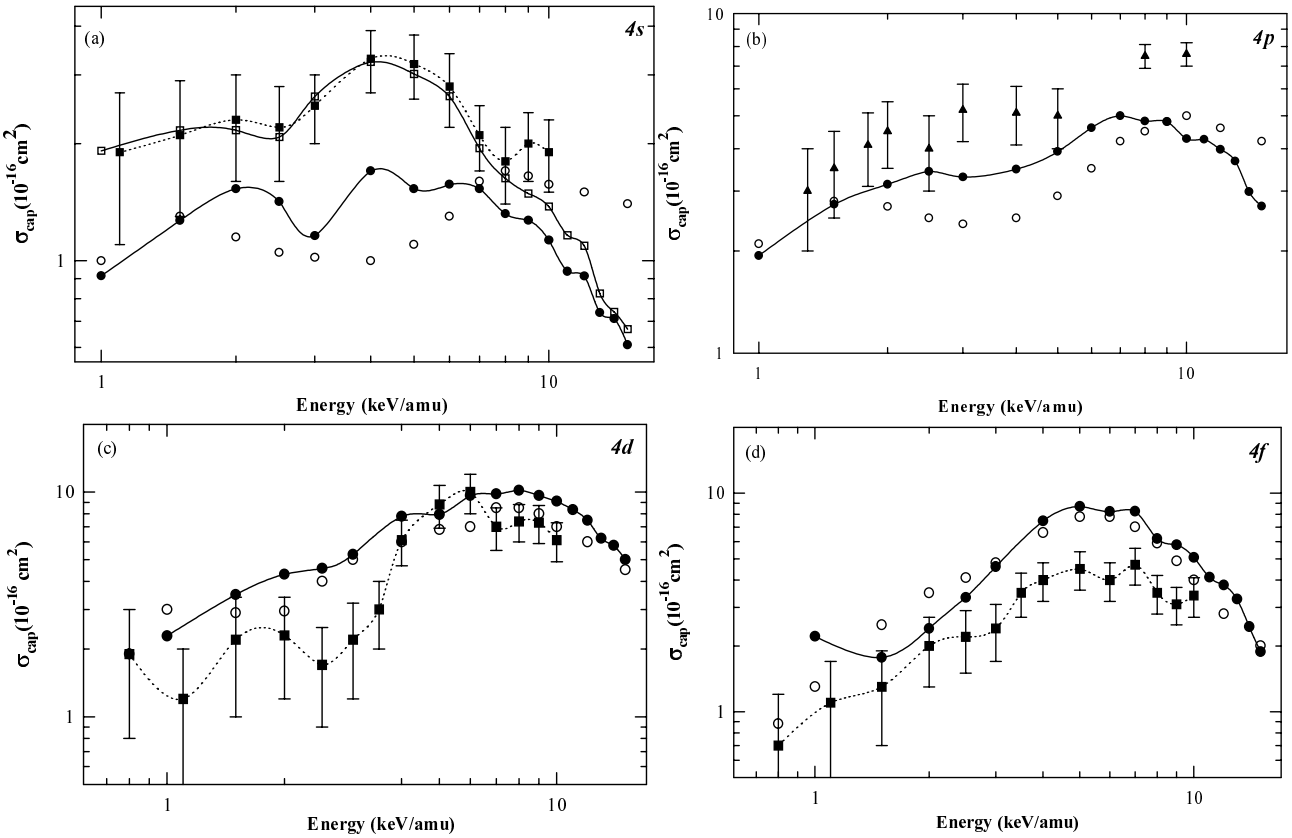

Fig. 2. Electron capture cross-section into $He^+(4l)$ states in He^{2+}–Li($2s$) collisions (a) $He^+(4s)$, (b) $He^+(4p)$, (c) $He^+(4d)$ and (d) $He^+(4f)$; (•: present CTMC result, ○: Fritsch and Lin [11] , ■: Hoekstra *et al.* [2], ▲: Dijkkamp *et al.* [27]) (in (a), □ denotes the apparent $4s$ cross-section determined from Eq. (5)).

that the respective capture cross-section does not change significantly [15,28]. The decrease in the Π cross-sections for the $4d$, $4p$ and $4s$ states as compared to that of $4f$ state is due to the decrease in overlap of Π state with the final projectile states. The Π state overlap with the $4s$ state is less than any other sublevel.

3.1.3 Oscillations in the partial cross-section

An interesting feature *viz.*; an oscillatory structure, has been observed in the partial cross-sections curve for both Li($2s$) and $Li^*(2p)$ targets. This kind of oscillatory structure has also been observed by several researchers in the total capture [29–34], partial capture [34,35], excitation and ionization [36,37] cross-sections and distinct models have been proposed towards its explanation. However, the identification of any explicit mechanism responsible for the observed structure is yet to crystallize.

The present CTMC undulatory structure very much resembles with that observed by Gieler *et al.* [32] in the case of H^+–(Li, Na, K) collisions. They have explained it in terms of interference effect between H($n = 2$) and the target excitation channels. Recently Krstic *et al.* [37] gave a complete quantum mechanical explanation for this oscillatory structure. They have argued that these oscillations have quantum mechanical origin and appear due to the interferences between phases of inelastic quasimolecular channels. Alternatively, these structures could well be a collective coherence phenomenon involving many states and, thus, could be explained, at least qualitatively by classical models [36]. A classical analog of this process has been proposed by MacAdam *et al.* [38] in which a transient molecular ion formation and the partially resolved contributions of one-, three- and higher-odd swap processes have been ascertained to cause these oscillations in case of ion-Rydberg atom collisions. The classical picture of quasi-molecular-ion formation has been illustrated by Ovchinnikov and Solov'ev [39] wherein they have shown to exist a specific topology corresponding to a specific range of internuclear distance for the classically allowed motion of an electron under the influence of both the target and projectile nuclei.

The velocity of the projectile being low in comparison to the orbital electron's velocity, the active electron gets a chance to move under the influence of both the cores for an appreciable time. This situation can well be described in terms of a transient quasi-molecule formation [40]. During the quasimolecular stage, the active electron undergoes a dangling (swapping [38] or multiple encounter [34]) between the two ion cores. This dangling motion of the active electron may end up in an excited state of either the projectile or the target or may leave both the cores leading

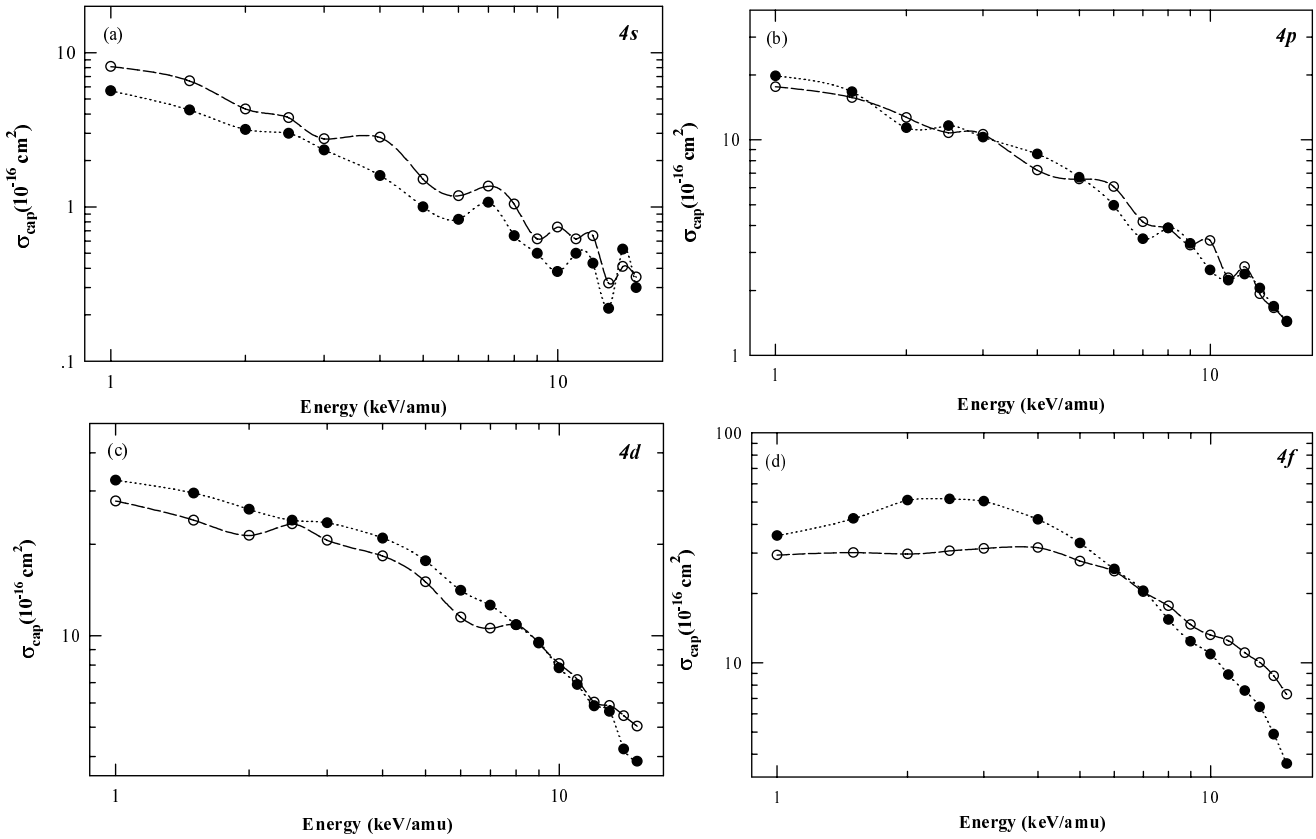

Fig. 3. Electron capture cross-sections into (a) $He^+(4s)$, (b) $He^+(4p)$, (c) $He^+(4d)$ and (d) $He^+(4f)$ substrates in He^{2+}–$Li^*(2p\Sigma, 2p\Pi)$ collisions; ($\circ$: $2p\Sigma$, $\bullet$: $2p\Pi$).

to the ionization of the target. Therefore, a similar structure should appear in the cross-sections not only for electron capture but also for excitation as well as ionization at similar impact energies. The oscillations noticed in the present ionization cross-sections therefore, support our reasoning given above (see Fig. 4). This explanation is also in consonance with that given in our earlier work [34] for understanding a more or less similar structure obtained in case of ion – Rydberg atom collisions. The present work therefore, further strengthens our proposal for quasi-molecular ion (QMI) formation [34] as another channel for the capture to take place. However, the oscillations appearing in the high energies (around 10 keV/amu) are in contrast with the structure found at the lower energies. Both, the formation of quasimolecule as well as the multiple interactions of the bound electron is not the likely processes at the high energies. These oscillations are therefore, due to the Thomas double encounter mechanism [41,42] which is a classical analog of quantum mechanical second order effects. Thomas proposed a double encounter mechanism as the dominant process at high collision speeds, in which the electron is first scattered by the impinging projectile at an angle around 60° with respect to the quantization axis. Subsequently, a second scattering by the target nucleus by another 60° deflects the electron in the forward direction with near zero velocity relative to the projectile leading to finally its capture. Higher order

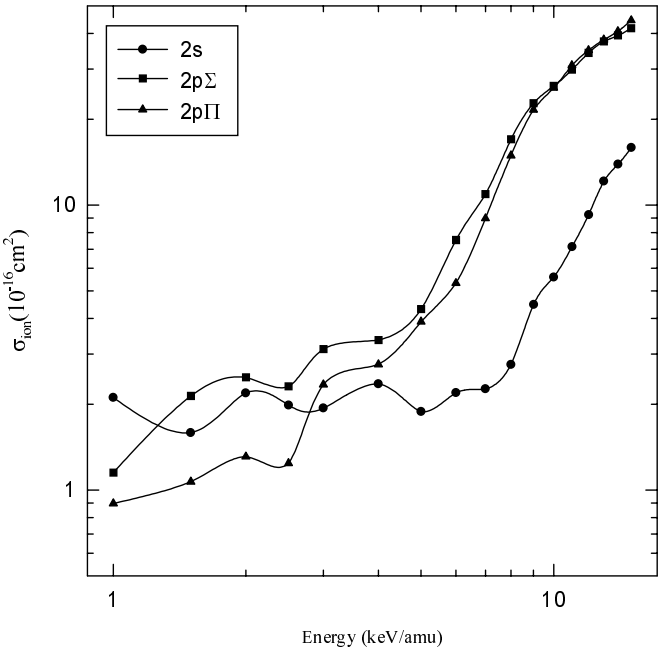

Fig. 4. Ionization cross-sections for the He^{2+}–$Li(2s, 2p\Sigma, 2p\Pi)$ collisions.

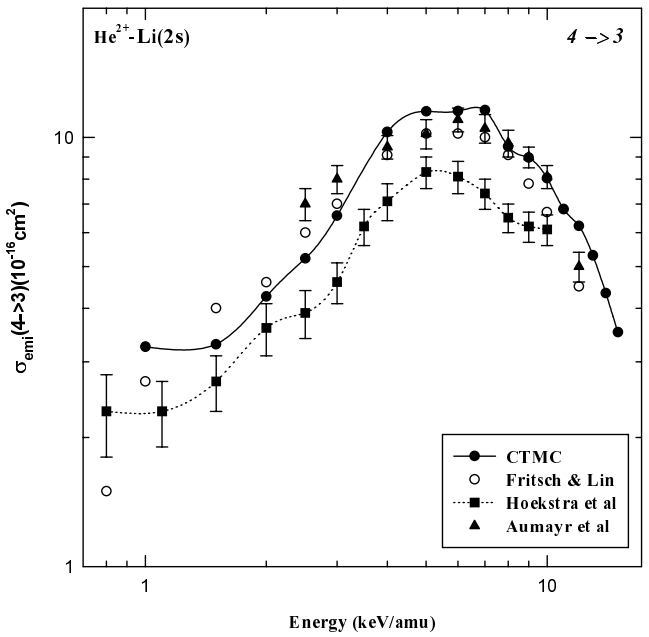

Fig. 5. Emission cross-sections for He II($4 \rightarrow 3$) with Li($2s$) as initial state.

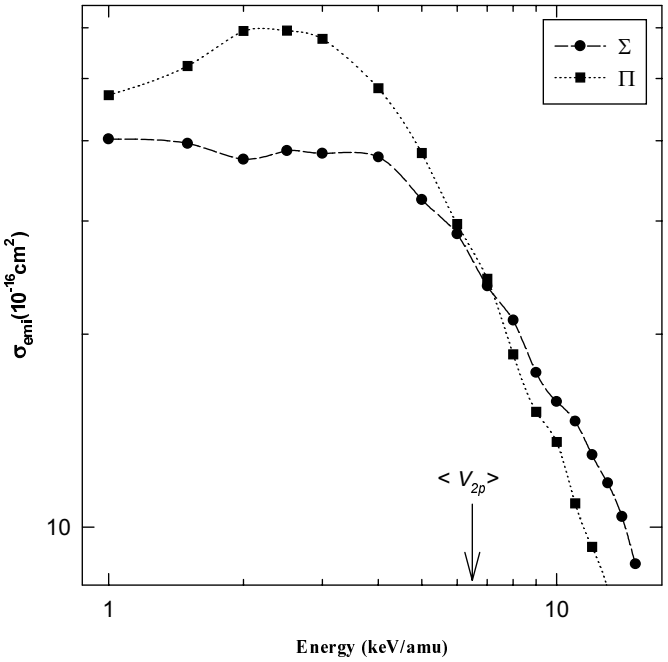

Fig. 6. Emission cross-sections for He II($4 \rightarrow 3$) with $2p\Sigma$ (•) and $2p\Pi$ (■) initial states. The arrow indicates the matching velocity (V_{2p}).

effects, if competitive, may further complicate the process of capture manifesting in oscillations of the capture cross-sections.

3.2 Line emission cross-section

Line emission cross-sections for $\Delta n = 1$ transition *viz.*; He II($4 \rightarrow 3$) have been determined for Li($2s$) target especially, to benchmark the present results with that of the measurements made by Hoekstra *et al.* [2]. Line emission cross-section has been determined using the $n = 4$ manifold of CTMC sublevel capture cross-sections and corresponding branching ratios (calculated from the transition probabilities in hydrogenic ions [43]). Summation over sublevels gives the total line emission cross-section for He II($4 \rightarrow 3$) transition *i.e.*,

$$\sigma_{\rm emi}(4 \rightarrow 3) = 0.416\sigma(4s) + 0.0417\sigma(4p) + 0.254\sigma(4d) + \sigma(4f). \quad (6)$$

This emission cross-section has been compared with the results of Hoekstra *et al.* [2], Aumayr *et al.* [12] and Fritsch and Lin [11] (see Fig. 5). CTMC cross-sections show an excellent agreement with the AO calculation and Aumayr *et al.*'s observed results. Hoekstra *et al.*'s observed line emission cross-sections are lower as compared to others including the present one.

The line emission cross-section for ($4 \rightarrow 3$) transition for Li*($2p\Sigma$, $2p\Pi$) targets have also been determined. The line emission cross-section with Π initial state is larger in magnitude ($\sim$ 50%) than that of the Σ state in the low energy region (Fig. 6). Both, the Σ and Π line emission cross-sections are equal at the velocity matching energy *i.e.*, $\sim$ 6.5 keV/amu. Above this the value of the Σ cross-section gradually increases over that of the Π cross-section. The reason for this behavior is also the same as the one given in case of the $4f$ sublevel capture cross-sections. The trend of the present line emission cross-section with incident energy is very similar to that of the observed one for He^{2+}–Na*($3p\Sigma$, $3p\Pi$) systems [15].

3.3 Alignment parameters

3.3.1 R parameter

In order to assess the target alignment effects a *dimensionless* parameter "R" in terms of the cross-sections of the excited Σ and Π orbitals relative to that of Li($2s$), have been defined [14] *viz.*;

$$R_\Sigma = \frac{\sigma_{2p\Sigma}}{\sigma_{2s}} \quad (7)$$

$$R_\Pi = \frac{\sigma_{2p\Pi}}{\sigma_{2s}} \quad (8)$$

where σ_{2s} and $\sigma_{2p\Sigma,\Pi}$ are the line emission cross-sections of He II($4 \rightarrow 3$) transition for the Li($2s$) and Li*($2p\Sigma$, Π) orbitals, respectively. Figure 7 shows the variation of the *dimensionless* parameters R_Σ and R_Π with the incident energy. The emission cross-section from the Li*($2p\Pi$) orbital, relative to the cross-section of Li($2s$), decreases monotonically (from 14 to 1.4) in a significant way over the entire energy range. The relative emission cross-section for electron capture from the Li*($2p\Sigma$) orbital, however, follows the same trend of Li*($2p\Pi$) below the matching velocity, but increases afterwards. The R parameter shows

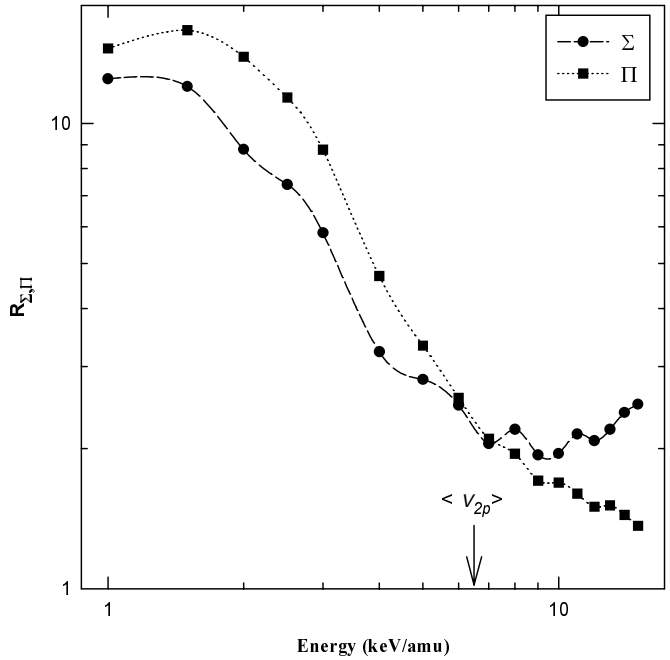

Fig. 7. Variation of dimensionless parameters R_Σ and R_Π for the He II($4 \rightarrow 3$) line emission (defined in Eqs. (7, 8)) with incident energy. The arrow indicates the matching velocity (V_{2p}).

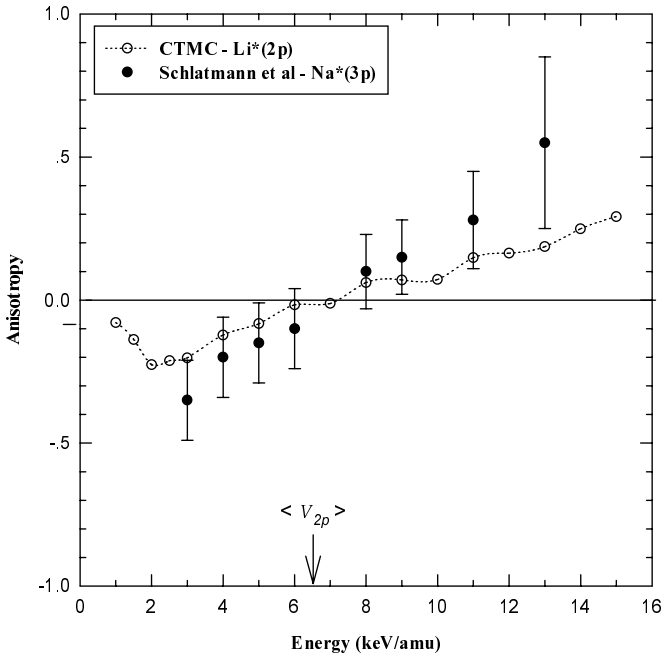

Fig. 8. Anisotropy parameter A for He II($4 \rightarrow 3$) line emission (defined in Eq. (9)) (○: present CTMC; ●: Schlatmann *et al.* for He^{2+}–$Na^*(3p)$ [15]). The arrow indicates the matching velocity (V_{2p}).

almost the same trend for both the Σ as well as Π states in the velocity matching region which reflects the fact that the cross-section at this energy is independent of the shape of the charge clouds. It is also seen from the figure that at velocity matching energy, $Li^*(2p)$ cross-section is ~ 2.5 times larger as compared to the $Li(2s)$ cross-section. In the lower energy regime the increase in $Li^*(2p\Pi)$ cross-section is due to the overlap of initial and final channels whereas, at high energies the $Li^*(2p\Sigma)$ cross-section dominates due to the velocity matching process (active electron has a velocity component parallel to the collision velocity). This variation of the cross-section with energy is similar to that of Müller *et al.* [14] for the H^+–$Na^*(3p)$ system.

3.3.2 Anisotropy parameter A

The *dimensionless* anisotropy parameter A, which quantifies the difference in He II($4 \rightarrow 3$) line emission cross-section for the Σ and Π–$Li^*(2p)$ orbital geometries is defined as

$$A = \frac{\sigma_{2p\Sigma} - \sigma_{2p\Pi}}{\sigma_{2p\Sigma} + \sigma_{2p\Pi}} \qquad (9)$$

where $2p\Sigma$ and $2p\Pi$ represent the $Li^*(2p)$ orbitals initially aligned parallel and perpendicular to the projectile velocity, respectively. At low energies the anisotropy parameter is negative (see Fig. 8). It gradually increases and becomes positive with the increase of energy. The anisotropy shows a shallow minimum around 2 keV/amu, where the difference between the Σ and Π cross-sections is the maximum. It assumes zero value ($A = 0$) around the velocity matching energy (*i.e.* ~ 6.5 keV/amu), which implies that near the matching velocity (V_{2p}) the Σ and Π target symmetries do not affect the capture process differently. Above this energy, A increases sharply and acquires a maximum positive value indicating thereby a preference for capture from $Li^*(2p\Sigma)$ orbital. The projectile energy and spatial overlap therefore, play a vital role in determining the alignment effects. In the absence of any other results we have compared these with that of the He^{2+}–$Na^*(3p\Sigma,\ 3p\Pi)$ collision system studied by Schlatmann *et al.* [15]. The trend of the present $Li^*(2p)$ and $Na^*(3p)$ results are very similar with each other.

4 Conclusions

CTMC is shown to be a suitable method for the determination of the line emission cross-section and alignment parameters for He^{2+}–$Li(2s,\ 2p\Sigma,\ 2p\Pi)$ systems. Present CTMC cross-sections are found comparatively closer to the experimental results than that of the AO calculations. The undulations observed in the cross-sections at low energies have been explained qualitatively in terms of quasi-molecular ion formation. However, the oscillation found at high energies are in contrast with that of low energies and are due to the higher order effects like Thomas double encounter process. The results of *dimensionless* parameters demonstrate the importance of alignment effects with the characteristic velocity and the spatial overlap dependencies.

The authors wishes to thank Prof. D.K. Rai and Prof. Jean Pascale for their encouragement and critical comments during the course of this work. We are indebted to the learned referee for suggesting equation (5) in order to have real comparison with the measured partial cross-sections for 4*s* level. One of the authors (A.N.P.) is grateful to CSIR, New Delhi for the financial support given in the form of a Senior Research Fellowship (Award No. 9/13(736)/95-EMR-I).

References

1. R.E. Olson, J. Pascale, R. Hoekstra, J. Phys. B **25**, 4241 (1992).
2. R. Hoekstra, E. Wolfrum, J.P.M. Beijers, F.J. de Heer, H. Winter, R. Morgenstern, J. Phys. B **25**, 2587 (1992).
3. E. Wolfrum, R. Hoekstra, F.J. de Heer, R. Morgenstern, H. Winter, J. Phys. B **25**, 2597 (1992).
4. R. Hoekstra, R.E. Olson, H.O. Folkerts, E. Wolfrum, J. Pascale, F.J. de Heer, R. Morgenstern, H. Winter, J. Phys. B **26**, 2029 (1993).
5. H. Ryufuku, K. Sasaki, T. Watanabe, Phys. Rev. A **21**, 745 (1980).
6. A. Niehaus, J. Phys. B **19**, 2925 (1986).
7. R.E. Olson, R. Hoekstra, Nucl. Instrum. Meth. B **98**, 214 (1995).
8. H. Winter, Comment. At. Mol. Phys. **12**, 165 (1982).
9. R.P. Schorn, E. Wolfrum, F. Aumayr, E. Hintz, D. Rusbüldt, H. Winter, Nucl. Fusion **32**, 351 (1992).
10. F. Aumayr, M. Gieler, J. Schweinzer, H. Winter, J.P. Hansen, Phys. Rev. Lett. **68**, 3277 (1992).
11. W. Fritsch, C.D. Lin, J. Phys. B **16**, 1595 (1983).
12. F. Aumayr, J. Schweinzer, H. Winter, J. Phys. B **22**, 1027 (1989).
13. C.J. Lundy, R.E. Olson, Nucl. Instrum. Meth. B **98**, 223 (1995).
14. U. Müller, H.A.J. Meijer, N.C.R. Holme, M. Kmit, J.H.V. Lauritsen, J.O.P. Pedersen, C. Richter, J.W. Thomsen, N. Andersen, S.E. Nielsen, Z. Phys. D **33**, 187 (1995).
15. A.R. Schlatmann, R. Hoekstra, R. Morgenstern, R.E. Olson, J. Pascale, Phys. Rev. Lett. **71**, 513 (1993).
16. S. Schippers, A.R. Schlatmann, W.P. Wiersema, R. Hoekstra, R. Morgenstern, R.E. Olson, J. Pascale, Phys. Rev. Lett. **72**, 1628 (1994).
17. M. Gieler, F. Aumayr, J. Schweinzer, W. Koppensteiner, W. Husinsky, H.P. Winter, K. Lozhkin, J.P. Hansen, J. Phys. B **26**, 2137 (1993).
18. J.W. Thomsen, Can. J. Phys. **74**, 950 (1996).
19. M. Gieler, F. Aumayr, M. Weber, H.P. Winter, J. Schweinzer, J. Phys. B **26**, 2153 (1993).
20. R.E. Olson, A. Salop, Phys. Rev. A **16**, 531 (1977).
21. A.N. Perumal, D.N. Tripathi, J. Phys. Soc. Jpn **66**, 3783 (1997).
22. H. Klapisch, C.R. Acad. Sci. Paris B **265**, 914 (1967).
23. I. Fourré, C. Courbin, Z. Phys. D 3**8**, 103 (1996).
24. A.N. Perumal, D.N. Tripathi, Phys. Lett. A **245**, 435 (1998).
25. R.C. Becker, A.D. Mackellar, J. Phys. B **17**, 3923 (1984).
26. C. Laulhé, E. Jacquet, P. Boduch, M. Chantepie, N. Ghérardi, X. Husson, D. Lecler, J. Pascale, J. Phys. B **30**, 2899 (1997).
27. D. Dijkkamp, A. Boellaard, F.J. de Heer, Nucl. Instrum. Meth. B **9**, 377 (1985).
28. S. Schippers, A.R. Schlatmann, R. Morgenstern, Phys. Lett. A **181**, 80 (1993).
29. F.J. Smith, Phys. Lett. **20**, 217 (1969).
30. C.F. Melius, W.A. Guddard III, Phys. Rev. A **10**, 1541 (1974).
31. F. Aumayr, G. Lakits, H. Winter, Z. Phys. D **6**, 145 (1987).
32. M. Gieler, F. Aumayr, P. Ziegelwanger, H. Winter, M. Fritsch, Phys. Rev. A **43**, 127 (1991).
33. R.K. Janev, J. Pop-Jordanov, E.A. Solev'ev, J. Phys. B **30**, L353 (1997).
34. A.N. Perumal, D.N. Tripathi, Nucl. Instrum. Meth. B **143**, 429 (1998).
35. D.M. Homan, K.B. MacAdam, M.J. Cavagnero, Phys. Rev. A **57**, R13 (1998).
36. D.R. Schultz, C.O. Reinhold, P.S. Krstic, Phys. Rev. Lett. **78**, 2720 (1997).
37. P.S. Krstic, C.O. Reinhold, D.R. Schultz, J. Phys. B **31**, L155 (1998).
38. K.B. MacAdam, J.C. Day, J.C. Aguilar, D.M. Homan, A.D. MacKellar, N.J. Cavagnero, Phys. Rev. Lett. **75**, 1723 (1995).
39. S. Yu, Ovchinnikov, E.A. Solov'ev, Sov. Phys. JETP **63**, 538 (1986).
40. J. Perel, Phys. Rev. A **1**, 369 (1970).
41. L.H. Thomas, Proc. Roy. Soc. **114**, 561 (1927) .
42. J. Wang, R.E. Olson, Phys. Rev. Lett. **72**, 332 (1994).
43. H.A. Bethe, E.E. Salpeter, *Quantum Mechanics of One- and Two-Electron Atoms* (Springer, Berlin, 1957).